Communications in Nonlinear Science and Numerical Simulation 118 (2023) 107012

Contents lists available at ScienceDirect

Communications in Nonlinear Science and Numerical Simulation

journal homepage: www.elsevier.com/locate/cnsns

Research paper

Geometric dynamics of anchored filamentous networks subject to viscous flow

Congping Lin [a], Peter Ashwin [b,*]

[a] School of Mathematics and Statistics, Center for Mathematical Sciences & Hubei Key Lab of Engineering Modelling and Scientific Computing Huazhong University of Science and Technology, Wuhan, China
[b] Department of Mathematics and Statistics, University of Exeter, Exeter, UK

ARTICLE INFO

Article history:
Received 20 January 2022
Received in revised form 30 October 2022
Accepted 9 November 2022
Available online 15 November 2022

Keywords:
Minimal networks
Geometric network dynamics
Endoplasmic reticulum

ABSTRACT

The Endoplasmic Reticulum (ER) is an organelle that can form a complex dynamic network of filaments embedded in the viscous flowing cytoplasm of plant cells, anchored to points in the cell membrane. We consider an idealized dynamical model of the ER network as constant tension filaments subject to viscous forces from cytoplasmic flow. We show that simple configurations lead to the creation of a filamentous network that is analogous to a 2D foam, but with different physical mechanisms. We consider a fixed set of anchor points and propose an adaptive algorithm to track the network in the presence of the flow. We find that minimal (Steiner) networks joining these anchor points can support filamentous network of varying geometries with and without an imposed flow. We demonstrate that, after the flow has ceased, the filamentous network can retain memory of previous flow direction and intensity.

1. Introduction

1.1. Endoplasmic Reticulumn Network Dynamics

Anchored networks consisting of fluid filaments under tension have direct application to understand Endoplasmic Reticulum (ER) networks in plant cells. The ER is the largest membrane-bound organelle in most eukaryotic cells, and spreads throughout the cytoplasm as one highly complicated inter-connected network that surrounds a single lumen. In particular, in plant epidermal cells, the ER lies within the thin layer of cytoplasm between plasma membrane and vacuole. The ER takes a variety of forms, one of which is a dynamic network of filaments [1–6] within the cytoplasm, anchored to the plasma membrane at various fixed locations or "anchors" (also called "terminals" or "persistent nodes" [2,7]). This "filamentous foam" or "filamentous network" evolves rapidly for a number of reasons: see [8] and Fig. 1. In living cells, the cytoplasm is a (complex non-Newtonian) fluid that can spontaneously flow as a result of active processes within the cytoplasm. In many practical purposes it can be modelling as a viscous flow [9]. Cytoplasmic streaming can make dramatic or gradual changes on ER network; cytoplasmic streaming typically evolves at a speed order of 1 μm/s [10]; movement of the streaming pattern evolves on a slow timescale compared to its streaming speed.

* Corresponding author.
E-mail address: P.Ashwin@exeter.ac.uk (P. Ashwin).

https://doi.org/10.1016/j.cnsns.2022.107012

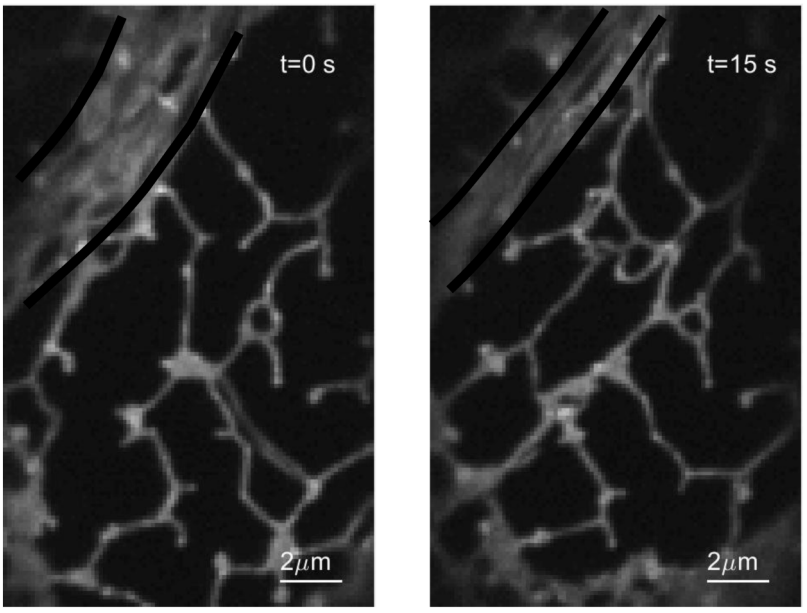

Fig. 1. Two frames from a movie illustrating ER network dynamics within a single tobacco leaf epidermal cell. The grey areas indicate the location of a fluorescent marker within the ER lumen taken 15 s apart. The network of ER filaments can be seen to move and reform under the influence of motion in the thin flat layer of cytoplasm and the filament tension. The regions between the black curves are regions of rapid streaming. (Reproduced with permission from [8, Fig. 1]. See also [8, Supplementary Movie 1].).

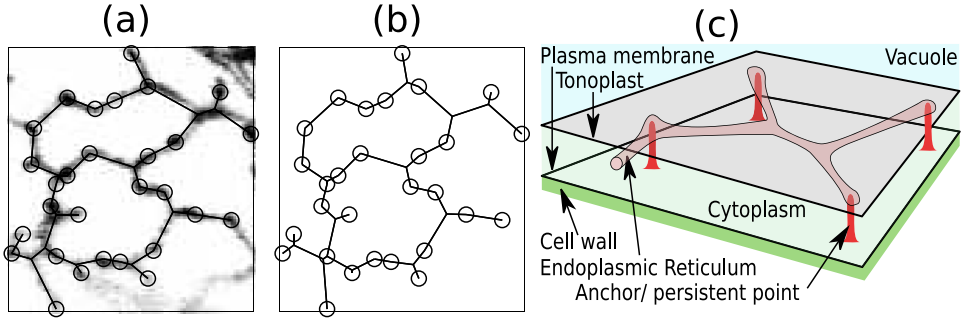

Fig. 2. (a) Diagram showing a small part of an experimentally inferred ER network plotted on top of an instantaneous image of the ER (shown here in negative relative to Fig. 1). (b) Nearby minimal network with the same terminals as (a). (c) Schematic of a portion of the ER filament confined to cytoplasm between plasma membrane and tonoplast and anchored by protein complexes [2] to the plasma membrane. Note the presence of internal junctions driven by tension forces, and the possibility of more than one stable configuration of ER joining the persistent points. We model the idealized behaviour of filamentous networks under the influence of cytoplasmic streaming ((a, b) are reproduced with permission from [4]).

1.2. ER and Euclidean Steiner Networks

Live cell imaging suggests that, away from regions of fast cytoplasmic streaming, the ER filamentous network is close to a local minimal length network ([7] suggests that the filaments have approximately uniform tension meaning the configuration can be modelled as a Euclidean Steiner Network (ESN) perturbed by Brownian and other forces). See Fig. 2(a) for an example of an ER network extracted from an experimental image. Fig. 2(b) shows a minimal length network connecting the anchoring points identified from the observed ER networks shown in panel (a); this ESN in panel (b) is close to experimental ER shown in panel (a). If we consider a fixed set of anchors $u_1, \ldots, u_p$ in $\mathbb{R}^2$, an ESN is a network connecting these anchors (possibly including extra nodes $x_1, \ldots, x_M$ called as Steiner points) such that the network has minimal length under small perturbations of Steiner points that connect the same anchors, even when splitting is allowed [7]. This generalizes the notion of Steiner Tree (ST) [11]. As there can be several STs between a set of anchors and these differ in topology, there can be several possible ESNs connecting the same anchors. In contrast to a ST, an ESN can contain nontrivial cycles if it is not a global minimum in length. For up to three anchors, there is a unique ESN (which is also a ST). For small networks even with as few as four anchors, two or more ESNs are possible. Indeed, the simplest case of multiple STs appears for four anchors located at the vertices of a square; see Fig. 3. It is possible to support ESNs

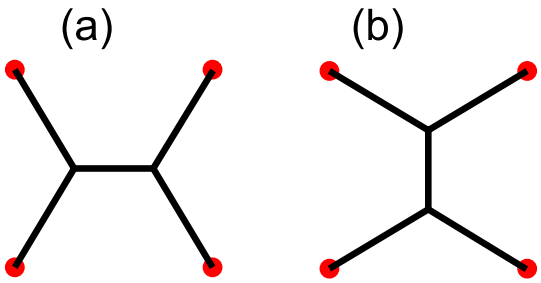

Fig. 3. Illustration of two possible Steiner trees on the plane between four anchors (red) at vertices of a square.

that are not STs with six anchors (see [7]). One property of STs or ESNs is that angles at 3-way junctions are 120° while angles at persistent points are no less than 120°.

In this paper, we model the behaviour of such networks anchored to simple viscous flows. We find that the combination of flows and multistability of (locally) anchored minimal networks lead to the development of filamentous networks that retain "memory" of the previous flow direction in the form of anisotropy of the structure. One can think of the cytoplasm/ER as a multiphase fluid, for there is an extensive literature on bubbles, foams and the role of surface tension (see for example [12]) which highlights the complexity of phenomena that can appear. In this paper we consider the behaviour of filamentous networks which are analogous to the well-studied 2D foams, but with rather different underlying physics.

2. Geometric dynamics of anchored filament networks

2.1. Motion of filaments between junctions

We model the motion of filaments between junction points and/or fixed anchors. Consider each point $\mathbf{x} = (x(l,t), y(l,t))$ parametrized smoothly by $l \in \mathbb{R}$ along the filament and time $t \geq 0$. Recall that if $x' := \frac{\partial x}{\partial l}$ and $y' := \frac{\partial y}{\partial l}$ at fixed t then the unit tangent and unit normal are

$$\mathbf{T}(l,t) = (x', y')/(x'^2 + y'^2)^{1/2},$$
$$\mathbf{N}(l,t) = (-y', x')/(x'^2 + y'^2)^{1/2}$$

respectively, and the unsigned curvature is

$$\kappa(l,t) = |x'y'' - y'x''|/(x'^2 + y'^2)^{3/2}.$$

The vector curvature is $\mathbf{K} = \pm\kappa\mathbf{N}$ with sign chosen in direction of curvature. Although the parameterization l does not need to be arc length, we assume that $|\mathbf{x}'| = \left|\frac{\partial \mathbf{x}}{\partial l}\right|$ is non-zero everywhere so that $\mathbf{T}$, $\mathbf{N}$, $\mathbf{K}$ and $\kappa \geq 0$ are well-defined.

Suppose that a filament (tubule) is moving in a moving medium with velocity field $\mathbf{v}(\mathbf{x}, t)$ (in unit of μm/s). This generates a drag force where we assume a constant drag coefficient σ per unit length of tubule, with units $\mathrm{N}\cdot\mathrm{s}/\mu\mathrm{m}^2$. Note that $\sigma \approx 4\pi\mu_v \log(L/r)$ for Stokes flow around a circular cylinder of length L, radius r and viscosity μ_v, if the cylinder axis is perpendicular to the flow [13]. We ignore this weak dependence on L and, given the curvature and unsteady flow, suggest a constant value for σ as a reasonable approximation [14].

We assume a constant tension coefficient τ (in unit of Newtons, N) along the tubule. By balancing the drag force and tension force (which is proportional to the curvature), we have (in unit of $\mathrm{N}/\mu\mathrm{m}$)

$$\sigma\left(\mathbf{v} - \frac{\partial}{\partial t}\mathbf{x}\right)\cdot\mathbf{N} = \tau\mathbf{K}\cdot\mathbf{N}. \tag{1}$$

Note that Eq. (1) does not specify the motion along the filament, corresponding to a re-parameterization of the filament by l. Indeed, $\mathbf{x}$ satisfying Eq. (1) will typically move according to

$$\frac{\partial}{\partial t}\mathbf{x} = v_N\mathbf{N} - \frac{\tau}{\sigma}\mathbf{K} + \alpha\mathbf{T} \tag{2}$$

where $v_N := \mathbf{v}\cdot\mathbf{N}$ is the velocity component in normal direction and α is an arbitrary function of l and t. For illustration, we use $\tau/\sigma = 1\ \mu\mathrm{m}^2/\mathrm{s}$ in all numerical simulations. We do not consider the motion along the filament, and instead we consider motion in the normal direction; thus we ignore the term $\alpha\mathbf{T}$.

2.2. Network dynamics in a viscous flow

Now consider a number of filaments in a viscous flow, where each filament ends either at an anchor or at a junction with two or more other filaments. If two filaments meet at an anchor they can interact. In particular, if the filaments meet at an angle less than 120°, the tension forces will pull out a new filament and create mobile three-way junctions to minimize the local filament length, as observed in ER remodelling [8].

We assume that mobile three-way junctions of filaments also move according to tension and viscous drag forces and that the filaments retain the same diameter by accessing a reservoir of material at each anchor. The motion of junctions is as in [8], namely a balance of surface tension and stokes drag force. More specifically, we assume the location $\mathbf{x}(t) \in \mathbb{R}^2$ of a junction point surrounded by three points moves according to

$$\frac{d}{dt}\mathbf{x} = b\Gamma \tag{3}$$

where $\Gamma := -\sum_{i=1}^{3} \mathbf{r}_i$ is the resultant geometric force over directions given by $\mathbf{r}_i$ the unit tangent vector at the junction $\mathbf{x}$. Considering a small neighbourhood of the junction, $b \approx \tau/(\sigma r)$ is an effective drift coefficient, where r is the diameter of the filament. In contrast to [8] we consider the limit of r small and specify a drag per unit length — this means we consider a singular perturbation r small. We remark here that the impact of Brownian motion is measurable but a perturbation to the changes of the ER caused by streaming [8], and thus we ignore the Brownian motion here.

We simulate the network of filaments using through cycles of the following steps: (a) Meshing filaments into line segments. (b) *Movement* of filaments according to Eq. (2). The non-persistent three-way junctions move according to tension and viscous drag only. (c) *Merging* any nodes that collide. (d) *Splitting* nodes if the angle at anchors (of degree 2) is less than $2\pi/3$ or if four or more filaments meet at a junction. We remark that four filaments may meet at a junction through the merging process. For the ER networks discussed in [8] it seems that the networks are maintained through a process of occasional *Cross linking* where filaments are added via actin-based processes at random locations in the network; we do not consider cross linking under flow here for simplicity.

More explicitly, we simulate filament networks described by these processes on a finite domain with periodic boundary conditions using an adaptive grid along the filaments. We discretize an initial network of filaments by splitting each filament into segments of length at most $\eta_{\max}$. We set maximal and minimal lengths $0 < \eta_{\min} < \eta_{\max}$ for the line segments, a threshold $\epsilon > 0$ for merging and a time step dt. For the time evolution of a filament network, we update the entire network of filaments by cycling through the following steps:

- **Splitting** We check the angles at the anchors and degree-4 points. If there is an angle of less than $2\pi/3$, then we split the vertex point and create a new point along the bisector of the angle at a distance ϵ. This is repeated until there are no more angles smaller than $2\pi/3$ for degree-2 anchors and degree-4 points.
- **Meshing** We mesh straight lines connecting filaments to ensure the each line segment is no larger than $\eta_{\max}$. More specifically, if one straight line has length larger than $\eta_{\max}$, then we add a new point in the middle of the line and repeat this process until all line segments have length no larger than $\eta_{\max}$.
- **Movement** We move degree 2 mesh-points along a filament as in Eq. (2) where in discretization, $\mathbf{N}$ and $\mathbf{K}$ are calculated from neighbouring points. Suppose two neighbours of $\mathbf{x} = P_2$ (w.l.o.g. one assumes $P_2 = (0, 0)$) are $P_{1,3}$ with coordinate $(x_{1,3}, y_{1,3})$. Denote the circumcentre as O. We then calculate $\mathbf{K}$ as

  $$\mathbf{K} = \frac{\overrightarrow{OP_2}}{|OP_2|^2} = \frac{2(x_1y_3 - y_1x_3)\mathbf{M}}{|P_1 - P_2|^2|P_1 - P_3|^2|P_2 - P_3|^2}$$

  where

  $$\mathbf{M} := \begin{pmatrix} y_1|P_3|^2 - y_3|P_1|^2 \\ -x_1|P_3|^2 + x_3|P_1|^2 \end{pmatrix}.$$

  We remark here that $\mathbf{K}$ is well defined as long as the three nodes $P_{1,2,3}$ do not overlap. A choice of the normal in the same direction as $\mathbf{K}$ is $\mathbf{N} = \overrightarrow{OP_2}/|OP_2|$. We relax degree-3 junctions at $\mathbf{x}$ towards balanced tension forces by time-stepping according to Eq. (3).
- **Merging** We merge two points connected by a line segment to one of the two points if they are no farther than $\eta_{\min}$ apart. We also rearrange connections if there is an intersection between two lines. More specifically, we create a new point at each intersection and merge the point closest to the intersection point.

For the simulations presented in this paper, we consider a domain of 20 μm$\times$20 μm with periodic boundary conditions in both directions, i.e. the topology of a torus. We set $\tau/\sigma = 1$ μm^2/s. Although we are interested in the case b large, we find that $b = 1$ μm/s, as used in [8], gives solutions with $|\Gamma| \ll 1$ except briefly after node splitting and so we use this value of b. We set $\eta_{\max} = 0.4$ μm; smaller $\eta_{\max}$ is used when necessary. We use $\eta_{\min} = 0.2 \times \eta_{\max}$ as the minimal segment length, $\epsilon = 2\eta_{\min}$ and a time step $dt = 0.0002$ s.

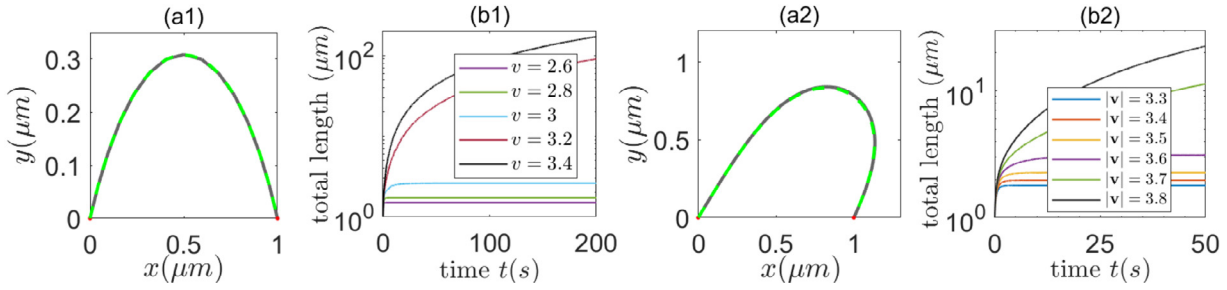

Fig. 4. (a1, a2) show examples of steady state filament under flow $\mathbf{v} = (0, 2)$ μm/s (a1) and $\mathbf{v} = (3.5\cos\pi/3, 3.5\sin\pi/3)$ μm/s (a2) respectively; red dots indicate anchors. The analytical solution given by Eq. (5) (dashed green curve) agrees well with numerical simulations (grey curves). (b1, b2) show the time evolution of total arc length for different flow $\mathbf{v} = (0, v)$ (b1) and $\mathbf{v} = |\mathbf{v}|(\cos\pi/3, \sin\pi/3)$ μm/s (b2) as indicated, with two anchors the same as in (a1, a2).

3. Results

We first study the dynamics of a network composed of uniform tension filaments under the influence of a viscous drag force from a background flow $\mathbf{v}$, with rules for reconfiguration at nodes. In the stationary case $\mathbf{v} = 0$ the network relaxes to an ESN. We explore some simple cases of this motion, in particular the existence of critical Capillary number beyond which filaments can grow unboundedly. This leads to the generation of highly nontrivial filament networks from quite simple initial networks of filaments. We then examine examples of phenomena that appear in small and large networks respectively. In particular, we highlight the apparent memory of flow direction in the resulting filamentous networks.

3.1. Single filament in a uniform flow

Consider a tubule between two anchors at $(x, y) = (0, 0)$ and $(x, y) = (L, 0)$ subject to a uniform steady flow. We choose to parameterize by the x-coordinate $l = x \in [0, L]$, and write the points on tubule as $(x, y(x, t))$. Then $\kappa = |y''|/(1+y'^2)^{3/2}$, and $\mathbf{N} = (-y', 1)/(1 + y'^2)^{1/2}$. In the simplest case $\mathbf{v} = (0, v)$ with $v > 0$ and seeking solutions where $y'' < 0$, Eq. (1) can be written as a PDE

$$\sigma(v + \dot{y}) = -\tau \frac{y''}{1 + y'^2} \tag{4}$$

with $\dot{y}$ denoting $\frac{\partial}{\partial t}y$ at fixed x. A steady solution to Eq. (4) reads as

$$y = \frac{1}{\nu} \ln|\cos(\nu(x + C_1))| + C_2, x \in [0, L] \tag{5}$$

where $\nu = \sigma v/\tau$, and $C_{1,2}$ are determined by boundary conditions: $y(0) = y(L) = 0$ and smoothness of $y(t)$; more precisely, $C_1 = \frac{2\pi - \nu L}{2\nu}$ and $C_2 = -\ln|\cos(vL/2)|/\nu$.

This steady solution $y(x)$ exists only for small enough Ca $:= |L\nu| = \left|\frac{Lv\sigma}{\tau}\right| \leq \pi$. The dimensionless quantity Ca is a Capillary number (a ratio of viscous to tension forces). If Ca is large enough for an anchored filament then there will 'bubble blowing': the arc length increases without bound until a re-connection happens. Fig. 4 (a1–b1) show that the analytical solution (5) for steady state curve agrees well with simulated curve and also that for flows with Ca $\leq \pi$ the filament has a stable total length, whereas with Ca $> \pi$ the filament length increases without bound.

Consider a filament between two anchors at $(0, 0)$ and $(a, 0)$ and under a flow in an arbitrary direction, say $\mathbf{v} = |\mathbf{v}|(\cos\theta, \sin\theta)$ with orientation of θ to the x-axis. Let a new coordinate system via anticlockwise rotating the $x - y$ coordinate by $\pi/2 - \theta$, $X = x\sin\theta - y\cos\theta$, $Y = x\cos\theta + y\sin\theta$. We note that with rotation of the coordinate, the curve in steady state under new coordinate $X - Y$ can be written in the form of Eq. (5), i.e.

$$Y = \frac{1}{\nu} \ln|\cos(\nu(X + \tilde{C}_1))| + \tilde{C}_2, \quad X \in [0, a\sin\theta] \tag{6}$$

where $\tilde{C}_{1,2}$ can be determined from fixed two anchors $(0, 0)$ and $(a\sin\theta, a\cos\theta)$ in $X - Y$ coordinate. Within the domain $X \in [0, a\sin\theta]$, for a steady solution we need $|a\nu\sin\theta| \leq \pi$, i.e. the Capillary number Ca $\leq \pi/|\sin\theta|$. We show an example for $\theta = \pi/3$ in Fig. 4 (a2–b2) that the analytical solution in Eq. (6) agrees well with the simulated curve and also that for a flow with the Capillary number Ca $= a|\mathbf{v}|\sigma/\tau \leq \pi/|\sin\theta|$, the filament has a stable total length, whereas for a flow with Ca $> \pi/|\sin\theta|$ the filament grows without bound.

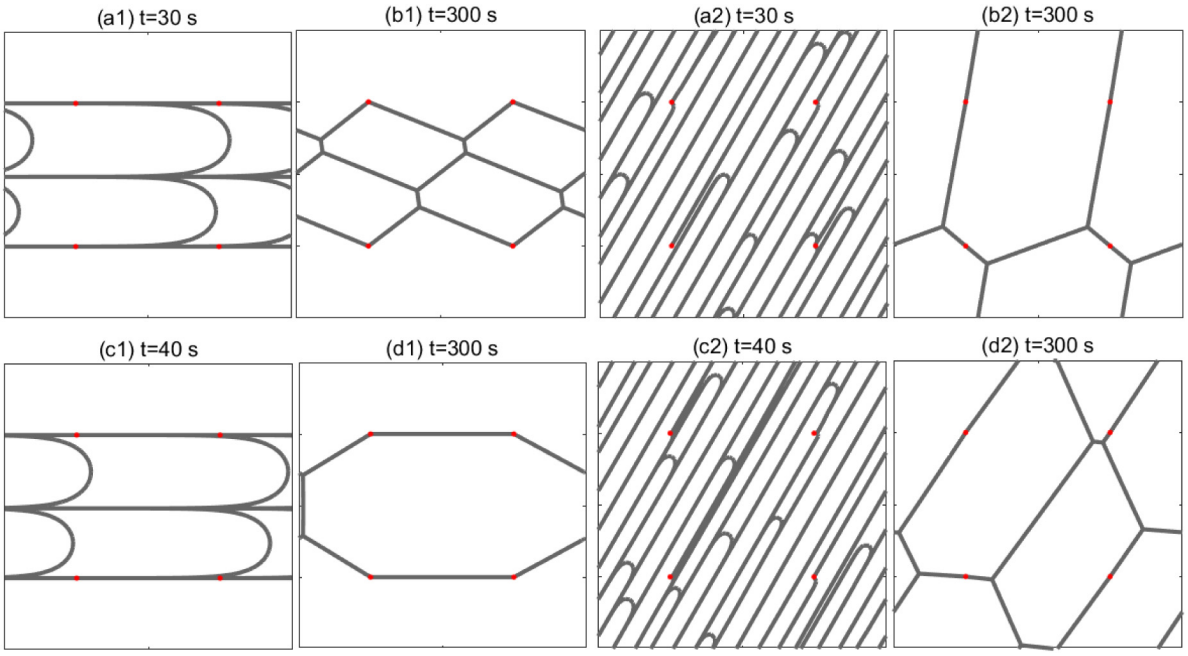

Fig. 5. Examples of filament network structure with streaming $\mathbf{v} = (5, 0)$ μm/s (a1, c1) and $\mathbf{v} = (5\cos\pi/3, 5\sin\pi/3)$ μm/s (a2, c2) starting with an initial network as in Fig. 3(b). Panels (b1, d1) show the relaxed network configurations after stream $\mathbf{v} = (5, 0)$ μm/s is ceased at configurations shown in panels (a1, c1) respectively. Similarly, panels (b2, d2) show the relaxed network configurations after stream $\mathbf{v} = (5\cos\pi/3, 5\sin\pi/3)$ μm/s is ceased at configurations shown in (a2, c2) respectively. Four anchors are indicated by red dots.

3.2. Flow memory retention in relaxed filamentous networks

In a stationary media note that the normal velocity to each filament is $v_N = 0$ in Eq. (2) and so if the network is also stationary we have $\frac{d}{dt}\mathbf{x} = 0$ which gives $\mathbf{K} = (0, 0)$. This means that $\kappa = 0$ and the filaments are straight lines. For 3-way junctions in a stationary network, we have $\Gamma = 0$ which indicates angles between edges connecting at the same 3-way junction are $2\pi/3$ and these junctions are Steiner points. For edges connecting at the same degree-2 anchors or degree-4 nodes form angles less than $2\pi/3$, nodes are split and new 3-way junctions form; these junctions move to be Steiner points or merge to other nodes. Eventually, networks relax towards ESNs.

For a network of filaments subject to steady streaming, if the Capillary number Ca for all filaments is sufficiently small then the filaments relax towards equilibrium curved filaments. If the Capillary number Ca is large then filaments in a finite domain with a periodic boundary condition will grow and merge with other filaments to create bubbles (cycles) that continue to change dynamically. For four anchors in a square within the domain, two possible Steiner trees are shown as in Fig. 3. We apply streaming to the network shown in Fig. 3(b). Fig. 5 shows that for $\mathbf{v} = (5, 0)$ μm/s and $\mathbf{v} = (5\cos\pi/3, 5\sin\pi/3)$ μm/s respectively, "bubbles" form through reconnections. Filaments in the network tend to be aligned in the orientation of the flow, even after stream is ceased. The relaxed networks after streaming is ceased retain the bubbles and tend to align with stream orientation, as seen from Fig. 5. The relaxed forms can be different, depending on network configurations at the time when streaming is ceased; see Fig. 5 (b1, d1, b2, d2). One could say that the relaxed network retains "memory" of past flow.

We investigate flow memory effects for large networks. Using a density of anchors 0.27 per μm^2 [8], we place $N = 108$ anchors at uniform independent random points in the domain 20 μm × 20 μm. Fig. 6 shows examples of initial and relaxed network configurations after streaming is ceased; the filamentous network undergoes streaming $|\mathbf{v}| = 5$ μm/s in directions of $\theta = 0$, $\pi/4$ and $\pi/2$ respectively until $t = 10$ s and then the network is relaxed driven by tension for 40 s (see Movie S1 for the network dynamics with an streaming orientation $\theta = 0$). Note that the relaxed network configurations (Fig. 6 (b1–b3)) show abundant filaments aligned with streaming direction. To test this quantitatively, we calculate distributions of filament segment angles weighted by segment length for both initial and relaxed networks. Fig. 7(a) show that the weighted angles in the relaxed networks Fig. 6 (b1) are more concentrated near 0 than the corresponding initial ESN shown in Fig. 6(a); in fact, there are 54% and 80% of filaments that are within $[-\pi/4, \pi/4]$ for networks in Fig. 6 (a, b1) respectively. We simulate an ensemble of 10 initial ESNs for the same set of anchors that are randomly distributed in the domain and their weighted angle distributions for both initial and relaxed networks are shown in Fig. 7(b). Weighted angles in the initial ESNs do not have a clear alignment; whereas, weighted angles in relaxed networks after streaming are highly concentrated near 0. These suggest that the relaxed network configurations are preferentially aligned with streaming orientation.

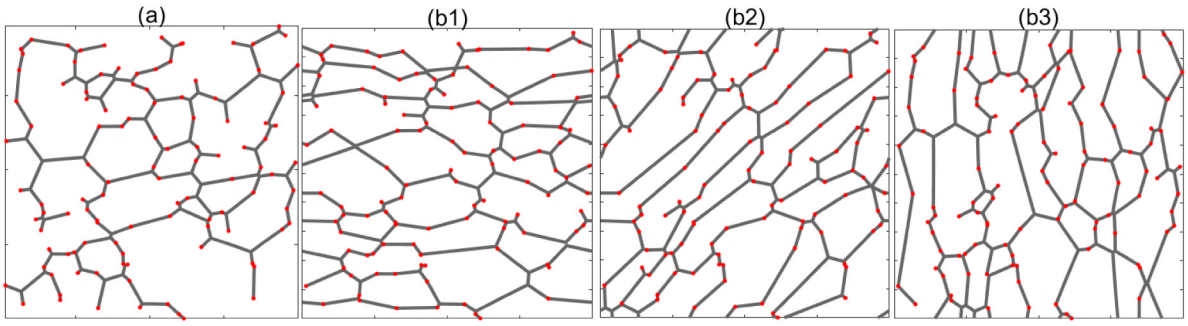

Fig. 6. Examples of filament network structures after streaming. (a) shows initial network structure; (b1–b3) are networks relaxed for 40 s after streaming is ceased at $t = 10$ s; the streaming speed is $v = |\mathbf{v}| = 5$ μm/s in a direction $\theta = 0$ (b1), $\theta = \pi/4$, (b2) and $\theta = \pi/2$ (b3). Red dots indicate anchors.

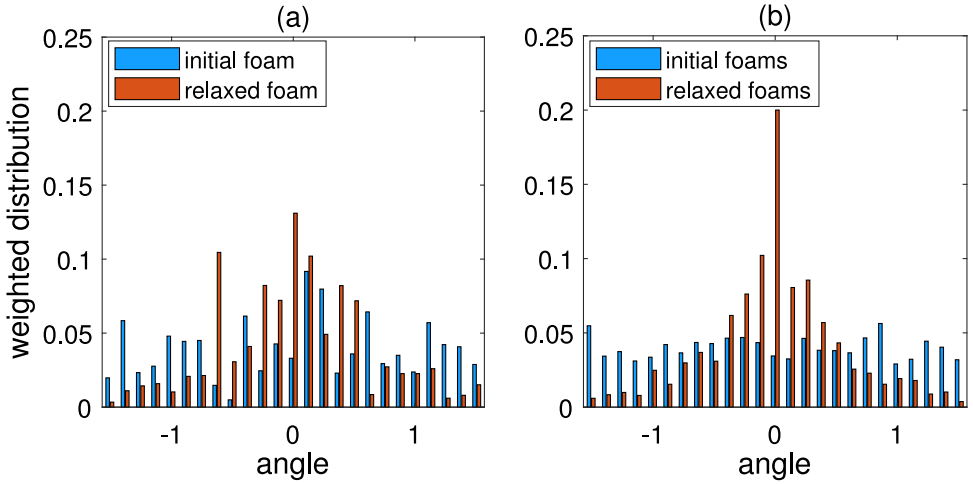

Fig. 7. Weighted angle distribution of filament segments from networks. (a) shows weighted angle distributions from an initial network in an ESN state shown in Fig. 6(a) and its evolved relaxed network configuration after stream $\mathbf{v} = (5, 0)$ μm/s as shown in Fig. 6 (b1). Angles are range from $[-\pi/2, \pi/2]$. (b) shows weighted angle distributions from 10 initial ESNs and their relaxed network configurations; each initial ESN has 108 anchors that are uniformly randomly distributed in the domain and is subject to a stream $\mathbf{v} = (5, 0)$ μm/s for 50 s and then relaxed for 100 s; anchors in the 10 initial ESNs are in the same locations.

For low velocity streaming, the relaxed filament network will retain the same topology as the original state. For large streaming, the relaxed network will increasingly align with the streaming direction. To quantify how the alignment degree depends on streaming speed, we calculate the proportion of aligned filament segments $P_t = \frac{L_{\theta,t}}{L_{\text{total},t}}$ for varying streaming speed $|\mathbf{v}|$; here $L_{\theta,t}$ is the total length of filament segments that are within $[\theta - \pi/4, \theta + \pi/4]$ for a given stream orientation θ and $L_{\text{total},t}$ is the total length of the filaments in the network at time t. After streaming is ceased the network relaxes to a steady configuration that is local minimal in total length. For initial sufficiently large number of anchors, if $|\mathbf{v}| \to \infty$, we expect $P_t \to 1 (t \to \infty)$ as filaments that are not aligned get "blown around". Without loss of generality, we consider $\mathbf{v} = (v, 0)$ (i.e. $\theta = 0$) and vary v for a domain 20 μm × 20 μm. Fig. 8 shows proportion and total filament length in the relaxed networks for varying v. Note that P fits reasonably well to an exponential equation $a_1 + (1 - a_1)(1 - \exp(-a_2 v))$. Also note that P is more or less constant for sufficiently small v as seen from Fig. 8(b) for $v = 0.01$ μm/s and $v = 0.1$ μm/s. Examples of the time evolution of P_t as well as total length of the network are shown in Fig. 8 (c, d). Note that for a large streaming speed, the proportion P_t and total network length reduces dramatically during a short time period immediately after stream is ceased.

In living cells, cytoplasmic streaming patterns typically evolve on a slow timescale, meaning the ER network interacts with a slowly varying streaming flow. We consider a simple example of this by rotating the streaming orientation at a constant rate while keeping the streaming speed fixed. We quantify the overall filament orientation in the network by the mean circular vector (mean circular vector angle Θ and length) [15] of filament segments weighted by segment length. Note that in filament networks, as the filament segments are unidirectional, we consider angles in a range of $(-\pi/2, \pi/2]$. Fig. 9 shows that for a large stream $v = 5$ μm/s, the mean weighted circular vector in networks is almost aligned with streaming orientation (also see Movie S2): the weighted mean circular vector angles are close to stream orientation and

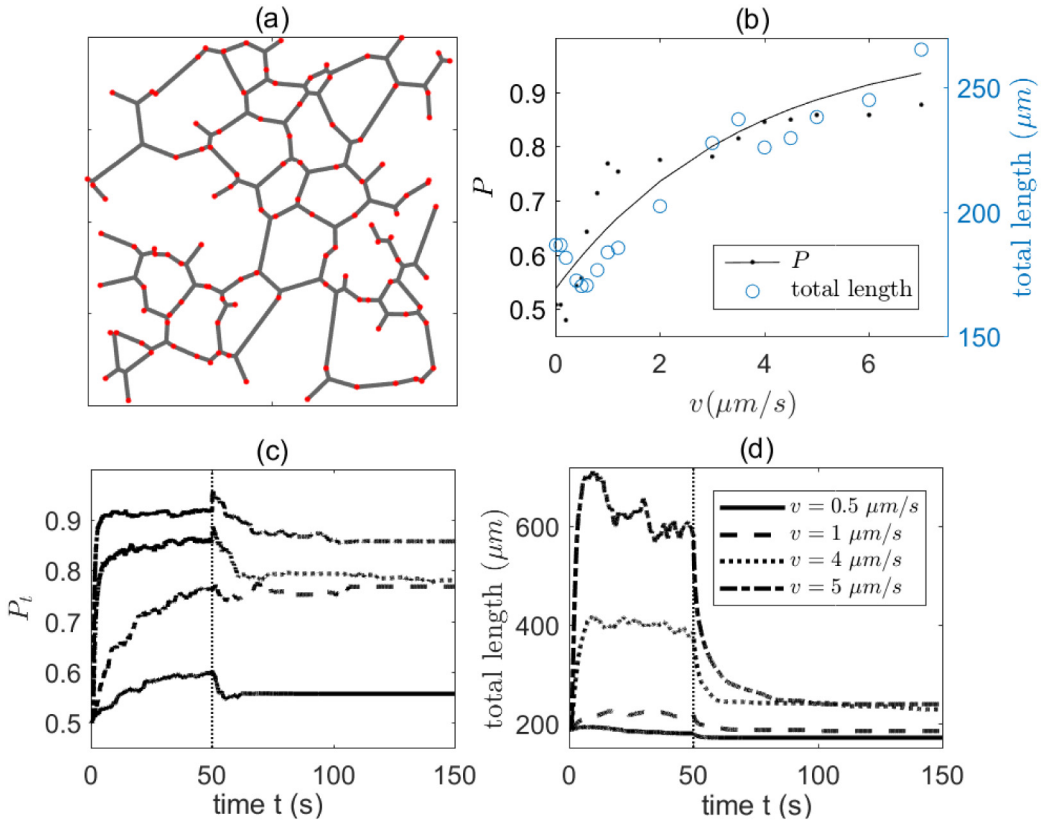

Fig. 8. (a) shows an initial graph in an ESN state. (b) shows the proportion (P, black) of line segments that are in alignment to stream direction (i.e. line segments in direction within $[-\pi/4, \pi/4]$ and the total filament length of the network (blue) after relaxed for 100 s for different streaming speed in horizontal. Black curve shows the exponential fit (with plateau=1, $R^2 = 0.84$) to the proportion in relation with stream speed v. Note that P is more or less constant for sufficiently small stream speed (e.g. $v = 0.01$ μm/s and $v = 0.1$ μm/s). (c) and (d) show the time evolution of proportion (P_t, c) and total filament length (d) with an initial network shown in (a) for different streaming speeds as indicated. Stream is ceased at $t = 50$ s for all simulations here.

the corresponding vector length is close to mean filament segment length during the network time evolution, except when the vector angles are around $\pm\pi/2$. Note that the drop of weighted mean circular vector length in Fig. 9(b) at stream angle around $\pm\pi/2$, is due to that approximately vertical filaments may assigned angles close $\pi/2$ or $-\pi/2$ considering the range choice $(-\pi/2, \pi/2]$ of unidirectional filament segment. Moreover, Fig. 9(a) also show that the proportion of weighted angles of filament segments aligned with streaming orientation is high. Overall, these suggest that for a high streaming speed, filament segments are highly aligned to streaming orientation. For a low streaming speed, filament segments are no longer aligned to stream direction as seen from the weighted mean circular vector as well as the proportion of weighted angles in aliment with stream direction as shown in Fig. 9.

4. Discussion

In conclusion, we find significant anisotropy of the 2D filamentous networks can be generated through steady streaming at a sufficiently high velocity. This flow memory effect means that even for a moderate number of random anchors, both direction and velocity can become encoded in the network state. It will be interesting to better understand the statistical mechanics of the resulting configurations and precisely which aspects of more complex flow patterns can also be committed to memory by such networks.

Our motivation for this study is the dynamics of ER networks in the living cell and their role in ER function [1]. There is frequent remodelling of the ER through both streaming and motor-driven processes. An obvious question is to what extent the remodelling is the aim of the streaming, and to what extent is the remodelling an unavoidable but unintended outcome of streaming? We remark that several additional aspects are present in the ER network that may be important to model, before considering more realistic geometries an spatial–temporal dependence for the cytoplasmic flow. In particular, the uniform tension may be valid as ER filaments draw out material from cisternae. But this is likely to valid only up to some point; for example ER filaments may break during remodelling [16].

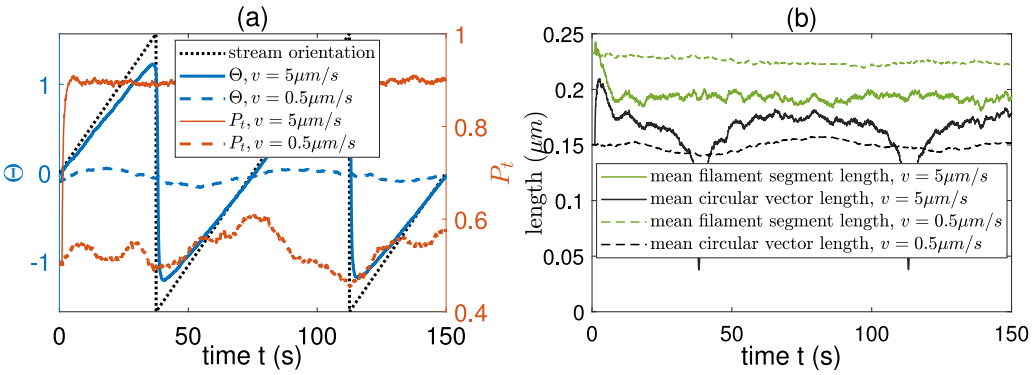

Fig. 9. (a) Left axis: time series of applied streaming orientation (dotted line) and mean weighted circular vector angles (Θ, blue) of filament segments from a model simulation. Right axis: proportion P_t (orange) of weighted angles of filament segments aligned with streaming orientation. Note that we consider angles unidirectional filament segment in a range of $(-\pi/2, \pi/2]$. (b) Time series of mean filament segments length (green) together with mean weighted circular vector length (black). Stream speeds $v = 5$ μm/s for solid lines and $v = 0.5$ μm/s for dashed lines are used.

Although some phenomena are similar to those found in 2D foams consisting of enclosed bubbles in 3D (in particular, the memory of applied strains in foam anisotropy [17–19]), the physics of our filamentous networks is quite different. In our case there is no pressure-driven force but rather a drag exerted by the streaming surrounding flow. In addition the pinning is to anchor points rather than boundaries. This means that, in the absence of streaming, a filamentous network will relax towards an anchored network of straight filaments connected by Steiner points.

CRediT authorship contribution statement

Congping Lin: Methodology, Writing – original draft, Writing – review & editing. **Peter Ashwin:** Methodology, Writing – original draft, Writing – review & editing.

Declaration of competing interest

The authors declare that they have no known competing financial interests or personal relationships that could have appeared to influence the work reported in this paper.

Data availability

The Matlab implementation is available at https://github.com/congping/filament-network-morphology-dynamics.

Acknowledgements

C.L. acknowledges financial support from National Natural Science Foundation of China (NSFC grant Nos. 12171179 and 11871061). This work was partially funded by Leverhulme Trust (RPG-2015-106). We thank Imogen Sparkes for introducing us to ER networks, for many insightful conversations and for permission to use the experimental data in Figs. 1 and 2, and we thank Graham Donovan for insightful conversations concerning this work.

Appendix A. Supplementary data

Supplementary material related to this article can be found online at https://doi.org/10.1016/j.cnsns.2022.107012.

References

[1] Westrate LM, Lee JE, Prinz WA, Voeltz GK. Form follows function: The importance of endoplasmic reticulum shape. Annu Rev Biochem 2015;84:791–811.
[2] Sparkes I, Hawes C, Frigerio L. FrontiERs: Movers and shapers of the higher plant cortical endoplasmic reticulum. Curr Opin Plant Biol 2011;14:658–65.
[3] Griffing LR, Gao HT, Sparkes I. ER network dynamics are differentially controlled by myosins XI-K, XI-C, XI-E, XI-I, XI-1, and XI-2. Front Plant Sci 2014;5:218.
[4] Griffing LR, Lin C, Perico C, White RR, Sparkes I. Plant ER geometry and dynamics: Biophysical and cytoskeletal control during growth and biotic response. Protoplasma 2017;254:43–56.
[5] Bouchekhima A-N, Frigerio L, Kirkilionis M. Geometric quantification of the plant endoplasmic reticulum. J Microsc 2009;234:158–72.

[6] Pain C, Kriechbaumer V, Kittelmann M, Hawes C, Fricker M. Quantitative analysis of plant ER architecture and dynamics. Nature Commun 2019;10:984.
[7] Lin C, Zhang Y, Sparkes I, Ashwin P. Structure and dynamics of ER: Minimal networks and biophysical constraints. Biophys J 2014;107:763–72.
[8] Lin C, White RR, Sparkes I, Ashwin P. Modeling endoplasmic reticulum network maintenance in a plant cell. Biophys J 2017;113:214–22.
[9] Niwayama R, Shinohara K, Kimura A. Hydrodynamic property of the cytoplasm is sufficient to mediate cytoplasmic streaming in the C. Elegans embryo. PNAS 2011;108:11900.
[10] Tominaga M, Kimura A, Yokota E, Haraguchi T, Shimmen T, Yamamoto K, et al. Cytoplasmic streaming velocity as a plant size determinant. Dev Cell 2013;27:345–52.
[11] Hwang FK, Richards DS, Winter P. The Steiner tree problem. North-holland; 1992.
[12] Lambert P. Surface tension in microsystems. Springer; 2013.
[13] Batchelor GK. Slender-body theory for particles of arbitrary cross-section in Stokes flow. J Fluid Mech 1970;44:419–40.
[14] du Roure O, Lindner A, Nazockdast EN, Shelley MJ. Dynamics of flexible fibers in viscous flows and fluids. Annu Rev Fluid Mech 2019;51:539–72.
[15] Mardia KV, Jupp PE. Summary statistics. John Wiley and Sons Ltd.; 2000.
[16] Sparkes IA, Ketelaar T, De Ruijter NC, Hawes C. Grab a Golgi: Laser trapping of Golgi bodies reveals in vivo interactions with the endoplasmic reticulum. Traffic 2009;10:567–71.
[17] Kraynik AM, Hansen Marion G. Foam rheology: A model of viscous phenomena. J Rheol 1987;31:175.
[18] Höhler R, Cohen-Addad S, Asnacios A. Rheological memory effect in aqueous foam. Europhys Lett 1999;48:93.
[19] Sessoms DA, Bissig H, Duri A, Cipelletti L, Trappe V. Unexpected spatial distribution of bubble rearrangements in coarsening foams. Soft Matter 2010;6:3030–7.